

THE EFFECT OF POROSITY ON X-RAY EMISSION LINE PROFILES FROM HOT-STAR WINDS

STANLEY P. OWOCKI

Bartol Research Institute, Department of Physics & Astronomy, University of Delaware, Newark, DE 19716

DAVID H. COHEN

Department of Physics & Astronomy, Swarthmore College, Swarthmore, PA 19081

Draft version July 27, 2018

ABSTRACT

We investigate the degree to which the nearly symmetric form of X-ray emission lines seen in *Chandra* spectra of early-type supergiant stars could be explained by a possibly porous nature of their spatially structured stellar winds. Such porosity could effectively reduce the bound-free absorption of X-rays emitted by embedded wind shocks, and thus allow a more similar transmission of red- vs. blue-shifted emission from the back vs. front hemispheres. To obtain the localized self-shielding that is central to this porosity effect, it is necessary that the individual clumps be optically thick. In a medium consisting of clumps of size ℓ and volume filling factor f , we argue that the general modification in effective opacity should scale approximately as $\kappa_{eff} \approx \kappa/(1 + \tau_c)$, where, for a given atomic opacity κ and mean density ρ , the clump optical thickness scales as $\tau_c = \kappa\rho\ell/f$. For a simple wind structure parameterization in which the ‘porosity length’ $h \equiv \ell/f$ increases with local radius r as $h = h' r$, we find that a substantial reduction in wind absorption requires a quite large porosity scale factor, $h' \gtrsim 1$, implying large porosity lengths $h \gtrsim r$. The associated wind structure must thus have either a relatively large scale $\ell \lesssim r$, or a small volume filling factor $f \approx \ell/r \ll 1$, or some combination of these. We argue that the relatively small-scale, moderate compressions generated by intrinsic instabilities in line-driving are unlikely to give such large porosity lengths. This raises questions about whether porosity effects could play a significant role in explaining nearly symmetric X-ray line profiles, leaving again the prospect of instead having to invoke a substantial (ca. factor 5) downward revision in the assumed mass-loss rates.

Subject headings: line: profiles — stars: early-type — stars: mass loss — stars: winds, outflow — X-rays: stars

1. INTRODUCTION

The high sensitivity and high spectral resolution of spectrometers on the *Chandra* X-ray observatory have made it possible to resolve X-ray emission line profiles from several hot, bright supergiant stars, e.g. ζ Pup, ζ Ori, δ Ori, ϵ Ori, ι Ori, ξ Per, and Cyg OB2 8A. [For an overview, see the introduction and discussion sections in Cohen et al. (2006).] The general broadness of these emission lines, with velocity half-widths of ca. 1000 km s⁻¹, is generally consistent with the idea that the X-rays are emitted in the expanding, highly supersonic stellar wind, perhaps from embedded shocks generated by instabilities associated with the line-driving of the overall wind outflow. However, these profiles are also generally quite symmetric¹ between the red and blue side, implying a small degree of attenuation of the red-side emission thought to originate in the back hemisphere relative to the observer.

In the standard wind-shock picture, the X-ray emission is believed to come from only a small fraction (< 1%) of the gas (Owocki, Castor, & Rybicki 1988; Feldmeier 1995; Feldmeier et al. 1997), with the bulk of the

wind consisting of relatively cool material with a substantial X-ray absorption opacity from bound-free transitions of helium and heavier ions. With the standard mass-loss rate for these stars, which are derived from either H α or free-free radio emission, the characteristic bound-free optical depths along a radial ray to the surface are expected to be of order ten or more (Hillier et al. 1993); since this implies a substantial attenuation of red-shifted emission originating from the back hemisphere, the expected X-ray emission line profiles have a markedly asymmetric form, with a much stronger blue side and a lower, more attenuated red side (Owocki & Cohen 2001, hereafter OC). Within a simple parameterized model, fitting the more symmetric observed profiles has thus required a substantial (ca. a factor 5 or more!) reduction in the assumed wind mass-loss rates (Kramer, Cohen, & Owocki 2003; Cohen et al. 2006). If confirmed, such a radical reduction in supergiant mass loss would have far-reaching consequences for both massive star evolution and the broad influence of wind mass loss on the structure of the interstellar medium.

This paper investigates an alternative scenario in which the reduction in wind attenuation might instead result from a spatially *porous* nature of the stellar wind. If wind material is compressed into localized, optically thick clumps, then red-shifted emission from the back hemisphere might be more readily transmitted through the relatively low-density channels or porous regions between the clumps.

Electronic address: owocki@bartol.udel.edu
cohen@astro.swarthmore.edu

¹ Actually, even for stars that have been qualitatively characterized as having symmetric X-ray line profiles, quantitative analyses (e.g., Cohen et al. 2006) show there is both a distinct blue-shift in the line centroid and a net skewness in the profile shape, albeit at levels much less than expected from standard wind models.

Feldmeier, Oskinova, & Hamann (2003) and Oskinova, Feldmeier, & Hamann (2004) have in fact examined such effects in quite detailed models that assume a specific ‘pancake’ form for the dense structures, under the presumption that these would arise naturally from the strong radial compressions associated with the intrinsic instability of the line-driving of such hot-star winds. Although 1D simulations of the nonlinear evolution of the instability do lead to compression into geometrically thin shells (Owocki, Castor, & Rybicki 1988; Feldmeier 1995), recent 2D models (Dessart & Owocki 2003, 2005) suggest the structure may instead break into clumps with a similarly small lateral and radial scale. But even such initial 2D simulations do not yet properly treat the lateral radiation transport that might couple material, and so the scale, compression level, and degree of anisotropy of instability-generated structure in a fully consistent 3D model is still uncertain.

This paper thus develops a simpler parameterized approach that aims to identify the basic properties needed for porosity to have a significant effect on the overall attenuation, and particularly to allow the near-symmetry of observed X-ray emission profiles. It builds on the simple parameterization developed by OC, which has been successfully applied to derive key wind properties needed to fit observed X-ray profiles under the assumption that absorption follows the usual (non-porous) form for a smooth wind (Kramer, Cohen, & Owocki 2003; Cohen et al. 2006).

Based on recent analyses of porosity effects in moderating continuum-driven mass loss (Owocki, Gayley, & Shaviv 2004), we present here (§2) simple scalings for the porosity reduction of effective opacity as a function of the optical thickness τ_c of individual clumps in a structured flow; for a given mean density and (microscopic) opacity, we show that this depends on the ratio of the clump scale ℓ to volume filling factor f , a quantity we dub the ‘porosity length’, $h \equiv \ell/f$. We next apply (§3) this scaling for porosity-modified opacity within the spatial integration for the wind optical depth, showing that, for a physically reasonable model in which this porosity length is assumed to increase linearly with local radius as $h = h'r$, the integral can be evaluated analytically (assuming also a canonical ‘beta=1’ form for the wind velocity law). We then use (§4) this analytic optical depth to compute X-ray emission line profiles for the simple case that the wind X-ray emission has a constant filling factor above some initial onset radius, set here to $R_o = 1.5R_*$, roughly where instability simulations show the initial appearance of X-ray emitting shocks, and roughly consistent with values derived by fits to the X-ray data. The discussion section (§5) then reviews implications of the key result that obtaining nearly symmetric profiles from an otherwise optically thick wind requires very large porosity lengths, $h \gtrsim r$, a requirement that seems at odds with the small scale and moderate compression factors found in instability simulations. The conclusion (§6) summarizes these results and briefly discusses the potential for future application of our porosity parametrization in spectroscopic analysis tools.

2. CLUMPING VS. POROSITY EFFECTS IN A STRUCTURED MEDIUM

2.1. Density-Squared Clumping Correction

Before discussing how porosity effects can alter diagnostics like bound-free absorption that scale linearly with density, it is helpful first to review briefly the usual account of how the clumping of a medium can alter diagnostics that scale with the *square* of the density. For example, emission and absorption from atomic states that arise from recombination, collisional excitation, or free-free processes all depend on the proximate interaction of two constituents, e.g. electrons and ions, and thus scale with the product of their individual particle density, e.g. $n_e n_i$, which for a fixed ionization and abundance is simply proportional to the square of the mass density, ρ^2 . The effect of spatial structure on such diagnostics is thus traditionally accounted for in terms of a simple density-squared clumping correction factor,

$$C_c \equiv \frac{\langle \rho^2 \rangle}{\langle \rho \rangle^2}, \quad (1)$$

where the angle brackets denote a volume averaging. For example, in a simple model in which the medium consists entirely of clumps of scale ℓ and mass m_c that are separated by a mean distance $L \gg \ell$, the mean density is $\langle \rho \rangle = m_c/L^3$, whereas the individual clump density is $\rho_c = m_c/\ell^3 = \langle \rho \rangle (L/\ell)^3$. Application in eqn. (1) then implies that the clumping correction is just given by the inverse of the volume filling factor,

$$C_c = \frac{L^3}{\ell^3} \equiv \frac{1}{f}. \quad (2)$$

For diagnostics of wind mass-loss rate, e.g. Balmer or radio emission, the associated overestimate in inferred mass loss scales as $\dot{M} \sim \sqrt{C_c} \sim 1/\sqrt{f}$.

A key point here is that this density-squared clumping correction depends only on the volume filling factor, $f = \ell^3/L^3$, and *not* on the scale ℓ of individual clumps. As long as the emission can escape from each local emitting clump (i.e., the clumps remain optically thin), the correction factor thus applies to structure ranging, for example, from very small-scale instability-generated turbulence (Dessart & Owocki 2003, 2005), to possible stellar-scale magnetically confined loops (ud-Doula & Owocki 2002).

2.2. Porosity Reduction in Linear-Density Opacity for Optically Thick Clumps

The attenuation of X-rays emitted within a stellar wind occurs through bound-free absorption, primarily from the ground-state. Since this is the dominant stage of the absorbing ions, and exists independent of interaction with other particles, the associated absorption scales only *linearly* with density, with the volume opacity (attenuation per unit length) given by $\chi = \kappa\rho$, where the mass opacity κ (mass absorption coefficient) has units of a cross section per unit mass, e.g. cm^2/g in CGS. Such linear-density absorption is often thought of as being unaffected by clumping.

If, however, we consider the above clump model in the case where the individual clumps are *optically thick*, then the ‘effective opacity’ of the clump ensemble can be written in terms of the ratio of the physical cross section of

the clumps to their mass,

$$\kappa_{eff} \equiv \frac{\ell^2}{m_c} = \frac{\kappa}{\tau_c} \quad ; \quad \tau_c \gg 1. \quad (3)$$

The latter equality shows that, relative to the atomic opacity κ , this effective opacity is reduced by a factor that scales with the inverse of the clump optical thickness, $\tau_c = \kappa \rho_c l = \kappa \langle \rho \rangle l / f$.

The above scaling serves to emphasize a key requirement for porosity, namely the *local self-shielding* of material within optically thick clumps, allowing then for a more transparent transmission of radiation through the porous interclump channels.

Note then that the clump optical thickness that determines the effective opacity reduction depends on the *ratio* of the clump *scale* to the volume filling factor, a quantity which we call the porosity length, $h \equiv \ell / f$. This represents an essential distinction between the porosity effect and the usual density-squared clumping correction, which as noted above depends only on the volume filling factor without any dependence on the clump size scale.

3. GENERAL POROSITY LAW BRIDGING OPTICALLY THIN AND THICK CLUMP LIMITS

To generalize the above effective opacity to a scaling that applies to both the optically thick and thin limits, consider that the effective absorption of clumps is more generally set by the geometric cross section times a correction for the net absorption fraction, $\sigma_{eff} = \ell^2 [1 - \exp(-\tau_c)]$. Applying this to modify the scaling in eqn. (3), we obtain a general porosity reduction in opacity of the form (Owocki, Gayley, & Shaviv 2004),

$$\frac{\kappa_{eff}}{\kappa} = \frac{1 - e^{-\tau_c}}{\tau_c}. \quad (4)$$

In the optically thick clump limit $\tau_c \gg 1$, this gives the reduced opacity $\kappa_{eff}/\kappa \approx 1/\tau_c$ of eqn. (3), while in the optically thin limit $\tau_c \ll 1$, it recovers the atomic opacity $\kappa_{eff} \approx \kappa$.

An even simpler, alternative bridging form can be derived by focussing on the effective mean path length within the medium, which scales with the inverse of the effective volume opacity, $1/\kappa_{eff} \langle \rho \rangle$. Within a model in which such an effective opacity adds in the inverse of contributing components (much as Rosseland mean opacity defined for weighting frequency-averaged opacity), we add the microscopic and clump components of path length as,

$$\frac{1}{\kappa_{eff} \langle \rho \rangle} = \frac{1}{\kappa \langle \rho \rangle} + h, \quad (5)$$

where we note that the porosity length defined above also defines a mean free path between clumps, $h \equiv \ell / f = L^3 / \ell^2$. This scaling solves to a general effective opacity of the form,

$$\frac{\kappa_{eff}}{\kappa} = \frac{1}{1 + \tau_c}. \quad (6)$$

This again gives both the correct scalings in the opposite asymptotic limits of optically thin vs. thick clumps. For moderately small clump optical depths $\tau \lesssim 1$, Taylor expansion shows the reduction is somewhat steeper for this new mean-path form of eqn. (6), i.e. as $1 - \tau_c$ instead of the slightly weaker $1 - \tau_c/2$ for the absorption scaling

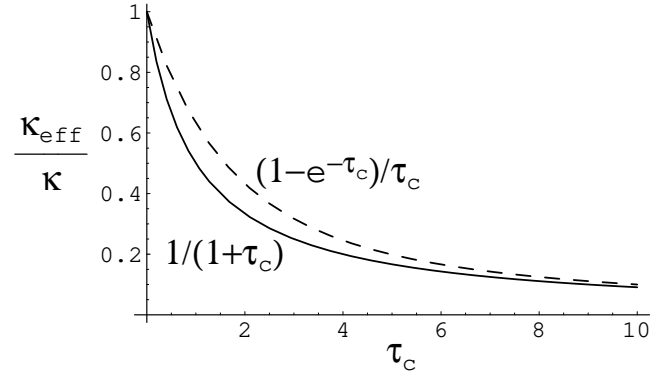


FIG. 1.— Comparison of absorption [dashed upper curve; eqn. (4)] and mean-path [solid lower curve; eqn. (6)] scalings of effective opacity in a porous medium, plotted as a function of clump optical thickness τ_c .

of eqn. (4). But the plot in Fig. 1 shows that both forms have a very similar overall variation with clump optical depth.

4. POROSITY EFFECT ON WIND OPTICAL DEPTH

The above formalism provides a convenient way to explore the effect of porosity on wind attenuation of X-ray emission. Our basic approach here is to generalize the parameterized analysis of OC to include the porosity reduction in effective absorption. For the effective opacity, we choose to work with the slightly simpler mean-path form (6), which avoids the complicating effects of the exponential function, with the clump optical thickness correction only appearing in a single linear term in the denominator. Following eqn. (OC-2), the effective optical depth to a position z along a ray with impact parameter p is now written as,

$$t_{eff}[p, z] = \int_z^\infty \frac{\kappa \rho[r']}{1 + \kappa \rho[r'] h[r']} dz', \quad (7)$$

where $\rho[r']$ is the smoothed-out mass density at radius $r' \equiv \sqrt{p^2 + z'^2}$, and $h[r']$ is the (possibly radially dependent) porosity length.

For a steady-state wind with a simple ('beta=1') velocity law of the form $w(r) \equiv v(r)/v_\infty = (1 - R_*/r) \equiv y(r)$, eqn. (7) becomes [cf. eqn. (OC-4)],

$$t_{eff}[p, z] = \tau_* \int_z^\infty \frac{R_* dz'}{r'(r' - R_*) + \tau_* h[r']}, \quad (8)$$

where, as in OC, we have here used the mass-loss rate, $\dot{M} \equiv 4\pi \rho v r^2$, to define a characteristic wind optical depth², $\tau_* \equiv \kappa \dot{M} / 4\pi v_\infty R_*$. As in eqn. (OC-4), for rays intersecting the core ($p \leq R_*$), eqn. (8) is restricted to locations in front of the star, i.e. $z > \sqrt{R_*^2 - p^2}$, since otherwise the optical depth becomes infinite, due to absorption by the star.

To account for the likely expansion of the clump size with the overall wind expansion, let us specifically assume here that the porosity length increases linearly with

² Note that in a smooth wind with a constant velocity $v = v_\infty$, the radial ($p = 0$) optical depth at radius r would be given simply by $t[0, r] = \tau_* R_*/r$. Thus in such a constant-velocity wind, τ_* would be the radial optical depth at the surface radius R_* , while $R_1 = \tau_* R_*$ would be the radius of unit radial optical depth.

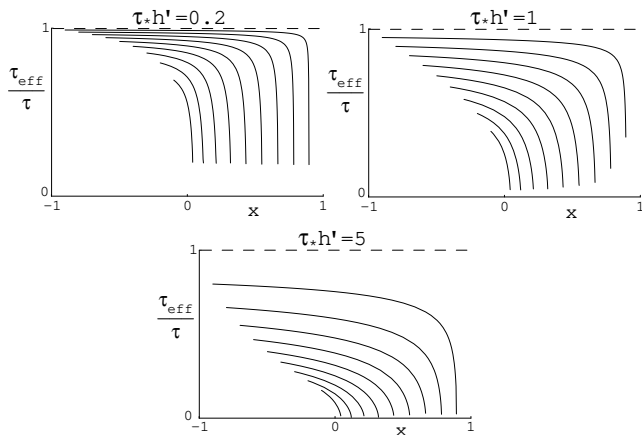


FIG. 2.— Ratio of the porosity-reduced effective optical depth to optical depth in a smooth wind, $\tau_{eff}[-x/w(r), r]/\tau[-x/w(r), r]$, plotted vs. the scaled wavelength x , at selected radii r in porosity models with $\tau_* h' = 0.2, 1, \text{ and } 5$ (left top to bottom panels). For each panel, the nine overplotted curves represent equal increments of scaled inverse-radius coordinate from $y \equiv 1 - R_*/r = 0.1$ to 0.9 , ordered from lower left to upper right.

the radius, i.e. as $h = h'r$. Fortunately, for this physically quite reasonable case, the integral in eqn. (8) can be evaluated analytically to give [cf. eqn. (OC-5)]

$$\frac{t_{eff}[p, z]}{\tau_*} = \frac{\left[\arctan\left(\frac{(1-\tau_* h')z'}{r'z_h/R_*}\right) + \arctan\left(\frac{z'}{z_h}\right) \right]_{z'=z}^{z' \rightarrow \infty}}{z_h/R_*}, \quad (9)$$

where $z_h \equiv \sqrt{p^2 - R_*^2(1 - \tau_* h')^2}$. In terms of the local direction cosine $\mu = z/r$, the effective optical depth as a function of spherical coordinates (μ, r) is given by

$$\tau_{eff}[\mu, r] = t_{eff}\left[\sqrt{1 - \mu^2} r, \mu r\right]. \quad (10)$$

At any given radius the projected Doppler shift from the wind velocity depends only on direction cosine μ . Thus, if we assume the intrinsic line profile of the local wind emission has a narrow, delta-function form, then upon integration over emission direction, we find a simple transformation from direction cosine to Doppler-shifted wavelength, $\mu \rightarrow -x/w(r)$, where $w(r) = v(r)/v_\infty = 1 - R_*/r$ is the scaled velocity law, and $x \equiv (\lambda/\lambda_o - 1)c/v_\infty$ is the Doppler shift in wavelength λ from line center λ_o , measured in units of the wind terminal speed v_∞ .

Figure 2 plots the porosity reduction in optical depth vs. wavelength x , for a selection of source radii r , with the panels from left top to bottom assuming increasing porosity, parameterized by $\tau_* h' = 0.2, 1, \text{ and } 5$. In the top-left panel, steep reductions only occur near those red-side wavelengths that, for the given source radius, require ray passage through the very inner wind, where the high density makes the clumps optically thick even for the modest assumed porosity length; since this generally means the overall optical depth in these regions is also quite high, the reductions still do not make the regions very transparent. But for the increasing porosity cases in the middle and lower panels, the reduction in optical depth occurs over a much broader range of wavelengths; these large porosity cases can thus indeed lead to a more transparent wind, with, as we now show, notable changes in the line profile.

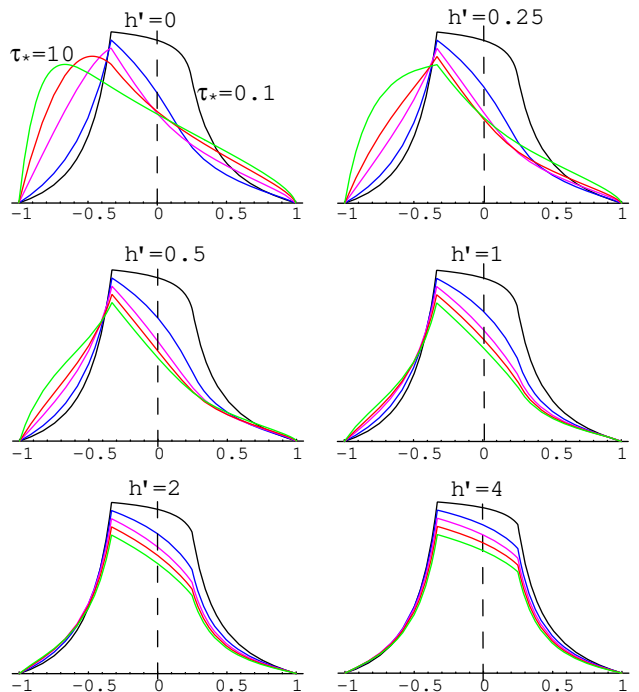


FIG. 3.— X-ray line profiles vs. scaled wavelength $x \equiv (\lambda/\lambda_o - 1)c/v_\infty$, overplotted in each panel for optical depth parameters $\tau_* = 0.1, 1, 3, 5, \text{ and } 10$ (black, blue, violet, red, green), and normalized to have peaks decrease by 5% for each step in τ_* . The panels compare results for various porosity scale factors $h' = 0, 0.25, 0.5, 1, 2, \text{ and } 4$, ordered from upper left to lower right. The vertical dashed line marks the line center. Note that porosity can make otherwise optically thick cases (i.e. $\tau_* = 3, 5, 10$) have nearly symmetric profiles, but only with quite large porosity scale factors, $h' > 1$, as seen in the lowermost panels.

5. POROSITY EFFECT ON X-RAY EMISSION LINE PROFILES

With the optical depths in hand, the computation of the emission line profiles follows directly the approach by OC. The wavelength-dependent X-ray luminosity can then be evaluated by straightforward numeral integration of a single integral in the scaled inverse-radius coordinate $y \equiv 1 - R_*/r$ [cf. eqn. (OC-9)],

$$L_x \propto \int_{y_x}^1 \frac{dy}{y^3} e^{-\tau_{eff}[-x/y, R_*/(1-y)]}, \quad (11)$$

where $y_x \equiv \max[|x|, 1 - R_*/R_o]$. For simplicity, we have assumed here that the X-ray emission filling factor is zero below a minimum X-ray emission radius R_o , and constant above this (i.e. the OC $q = 0$ case). Specifically, we assume here an X-ray emission onset radius of $R_o = 1.5R_*$, roughly where instability simulations show the appearance of self-excited wind structure with embedded shocks (e.g., Runacres & Owocki 2002), and roughly the favored value in detailed parameter fits to observed X-ray spectra (Kramer, Cohen, & Owocki 2003; Cohen et al. 2006).

Fig. 3 compares line profiles for various porosity scale factors, from the no porosity case ($h' = 0$; upper left) to large factors ($h' = 4$; lower right). Note that the profiles with large optical depth $\tau_* = 10$ (green curves, scaled to be the lowest in each panel) have strong blue-shifted asymmetry for cases with no or moderate porosity, ($h' \leq 1$), and approach the near symmetry of the

optically thin case ($\tau_* = 0.1$; black curves, scaled to have the highest peaks) only for models with very large porosity scale factor, $h' = 2$ or 4 (lowermost panels).

6. DISCUSSION

The basic result here is thus that, for cases with a large overall wind optical depth ($\tau_* > 2$), achieving a near symmetry in emission line profiles requires very large porosity lengths, $h \gtrsim r$. Since $h \equiv \ell/f$, this implies that the wind structure must either have a very large scale, $\ell \lesssim r$, or a small filling factor, $f < \ell/r$, or some combination of these.

It is interesting to compare this result with those obtained by Feldmeier, Oskinova, & Hamann (2003) and Oskinova, Feldmeier, & Hamann (2004) for their more specialized fractured-wind models that assume the line-driven instability will lead to radially compressed pancake structures separated by strong rarefactions. These authors have generally argued that the porous regions between such radially compressed structures could allow transmission of emission from the back hemisphere, and thus explain the greater-than-expected symmetry of observed X-ray line profiles. However, their most recent efforts (Oskinova, Feldmeier, & Hamann 2005) to obtain symmetric profiles with this model have typically assumed quite large radial separations between the dense compressions, on the order of a stellar radius or more.

This seems generally consistent with the requirement here for large porosity lengths. Indeed, in this picture of pancakes that arise from 1-D, radial compressions, the volume filling factor is just given by $f = \ell/L$, where ℓ is now the *radial* compression size of the pancakes, and L is the radial separation between them. Then using our definition for the porosity length, we see that in this case this porosity length is indeed just given by the separation scale, $h = \ell/f = L$. Moreover, if the pancakes are optically thick, this also gives a typical mean-free-path through the porous wind, much as in our description above. In both analyses, we see then that, for porosity to be sufficient to make the wind transparent, this mean path has to be quite large, comparable to or larger than a stellar radius.

Overall, these results thus raise serious issues for associating significant porosity reduction in X-ray absorption with the small-scale wind structure expected from the intrinsic instability of line driving. In linear analyses (e.g., Owocki & Rybicki 1984), this instability occurs for radial perturbations on the scale of the Sobolev length, $L_{Sob} = v_{th}/(dv/dr) \approx R_* v_{th}/v_\infty$; since typical wind terminal speeds of order $v_\infty \approx 1000$ km/s are much larger than the typical ion thermal speed $v_{th} \approx 10$ km/s, we find $L_{Sob} \approx 0.01R_*$. In 1D nonlinear simulations, this is indeed the typical scale of initial structure in the inner wind, with some subsequent outward increase due to merging as faster shells collide with slower ones (e.g., Feldmeier 1995; Runacres & Owocki 2002). But in 2D models (Dessart & Owocki 2003, 2005), individual clumps with different radial speeds can pass by each other, with shearing effects competing with merging, so that the typical scale remains quite small. In both 1D and 2D simulations, the net compression is found to be quite moderate, with associated volume filling factors typically of order $f \approx 0.1$. Thus to the extent that the complex structure can be characterized by a

single porosity length, it seems this would be of order $h = 0.01R_*/0.1 \approx 0.1R_*$, which is much smaller than what the above analysis suggests is necessary to give a substantial porosity effect on line profiles.

Of course, compared to the complex structure in such instability simulations, the above clump model is highly idealized and even simplistic, characterizing the structure in terms of a single size scale, and essentially assuming that the porous regions in between the isolated clumps are completely empty and thus transparent. But such simplifications would generally seem only to favor the development of porous transport, representing a kind of best-case scenario; it thus seems quite significant that even in this case the requirements for achieving a significant porosity are actually quite stringent.

The more extensive porosity analysis by Owocki, Gayley, & Shaviv (2004) suggests, for example, that in a medium with a distribution of clump scales, the porosity reduction in opacity scales with a weaker-than-linear power of inverse density, e.g. $1/\rho^\alpha$ for power-law distribution with positive index $\alpha < 1$, which reflects self-shielding as different scale clumps become optically thick. In their ‘inside-out’ context of porosity-mediated mass loss from dense layers of the stellar envelope, this modification tends to shift the wind sonic point to higher density, thus serving to increase the derived mass loss. But in the present ‘outside-in’ context of wind attenuation of X-rays seen by an external observer, the weaker scaling will only make it more difficult to give the outer regions near the X-ray photosphere a significant porosity reduction in absorption.

Thus, despite the simplicity of our basic model and analysis, we believe the central physical arguments are quite general and robust, indicating that significant porosity reductions in the absorption of otherwise optically thick winds are only possible for large porosity lengths $h \equiv \ell/f$, implying either quite large size scales ℓ , or strong compressions into a small filling factor f , or some combination of these. While large-scale structures may indeed exist in the winds of some specific stars, for example owing to global magnetic fields, the kind of ubiquitous structure expected from the intrinsic instability of line-driving seems simply to have too small a scale to play much role in porosity reduction of wind absorption.

Moreover, sufficiently large structure would seem likely to be associated with temporal variability of emergent X-rays due to, e.g., rotational modulation of the attenuation (in addition to likely modulations or even intrinsic variations in emission); but such variability is not generally seen in the X-ray spectra of hot stars, which are typically found to be constant to a level of a few percent or so (Berghoefer et al. 1996; Cohen et al. 1997). In addition, because magnetic fields generally retard or confine the wind outflow, leading to high-density structures (ud-Doula & Owocki 2002), their overall effect could even be an overall *increase* in absorption, relative to what would occur in a smooth, spherically symmetric wind outflow. Taken together, these considerations seem to argue against an important porosity effect from wind structure of any scale.

Of course, as extensively discussed in the literature, even small-scale, optically thin structure can have a major impact on diagnostics that scale with density-squared, leading for example to overestimates of the wind

mass loss that scale with $1/\sqrt{f}$. If mass-loss rates are thereby revised downward by significant factors of five or more, then it becomes possible to explain the observed near-symmetry of observed X-ray line-profiles in terms of reduced overall optical depths τ_* (Kramer, Cohen, & Owocki 2003; Cohen et al. 2006), without needing to invoke any porosity reduction in the effective opacity.

Mass loss reductions of this magnitude have in fact been recently suggested, based on NLTE models of hot star-spectra that include transitions with a mixed contribution from single-density and density-squared processes (Bouret et al. 2005), and based on FUSE observations of wind lines from a fuller range of ions spanning the dominant stage (Fullerton, Massa, & Prinja 2006). Such substantial reductions in hot-star mass loss would have broad-ranging implications, for example for massive-star evolution, and for the physics of the interstellar medium.

7. SUMMARY

We have carried out a simplified, parameterized analysis of the potential role of a porous medium in reducing the effective absorption of X-rays emitted in an expanding stellar wind. In contrast to the usual corrections for density-squared processes, which depends only on the volume filling factor, we show that the importance of such porosity effects depend largely on a quantity we call the porosity length, which is set by the ratio of the characteristic clump size scale to this filling factor. This determines the density and opacity for which the individual clumps become optically thick, leading to a local self-shielding within clumps that reduces the effective opacity

of the medium by a factor that scales with the inverse density. A key result is that porosity reduction of absorption at a level to make an otherwise optically thick line emission nearly symmetric requires very large porosity lengths, on order of the local radius or more, $h \gtrsim r$. Because a large porosity length requires a combination of large-size clump structures or a small, compressed filling factor, it seems unlikely that this could result from the small-scale, moderately compressed structure expected from the intrinsic instability due to line-driving. Despite the simplicity of the basic model, the key physical reasons for requiring large porosity lengths seem quite general and robust. An overall conclusion is thus that explaining the unexpectedly symmetric form for observed X-ray line-profiles may instead require substantial reductions in inferred mass-loss rates.

The parameterization developed here for the porosity reduction of opacity (see eqn. [6]) is simple enough to lend itself to general application within spectroscopic analysis codes like *XSPEC*. Future work on fitting observed spectra could then derive more specific requirements for porosity models to match line profiles, allowing one to explore further the trade-off between invoking porosity or lowering the wind mass-loss rate.

DHC acknowledges NASA contract AR5-6003X to Swarthmore College through the *Chandra* X-ray Center. SPO acknowledges NSF grants AST-0097983 and AST-0507581, and NASA/*Chandra* Theory grant GO3-3024C.

REFERENCES

- Berghoefer, T. W., Baade, D., Schmitt, J. H. M. M., Kudritzki, R.-P., Puls, J., Hillier, D. J., & Pauldrach, A. W. A. 1996, *A&A*, 306, 899
- Bouret, J.-C., Lanz, T., & Hillier, D. J. 2005, *A&A*, 438, 301
- Cohen, D. H., Cassinelli, J. P., & Macfarlane, J. J. 1997, *ApJ*, 487, 867
- Cohen, D. H., Leutenegger, M. A., Grizzard, K. T., Reed, C. L., Kramer, R. H., and Owocki, S. P. 2006, *MNRAS*, submitted
- Dessart, L. & Owocki, S. P. 2003, *A&A*, 406, L1
- Dessart, L., & Owocki, S. P. 2005, *A&A*, 437, 657
- Feldmeier, A. 1995, *A&A*, 299, 523
- Feldmeier, A., Kudritzki, R.-P., Palsa, R., Pauldrach, A. W. A., & Puls, J. 1997, *A&A*, 320, 899
- Feldmeier, A., Oskinova, L., & Hamann, W.-R. 2003, *A&A*, 403, 217
- Fullerton, A. W., Massa, D. L., & Prinja, R. K. 2006, *ApJ*, 637, 1025
- Hillier, D. J., Kudritzki, R. P., Pauldrach, A. W., Baade, D., Cassinelli, J. P., Puls, J., & Schmitt, J. H. M. M. 1993, *ApJ*, 276, 117
- Kramer, R. H., Cohen, D. H., & Owocki, S. P. 2003, *ApJ*, 592, 532
- Oskinova, L., Feldmeier, A., & Hamann, W.-R. 2004, *A&A*, 422, 675
- Oskinova, L., Feldmeier, A., & Hamann, W.-R. 2005, *astro-ph/0511019*
- Owocki, S. P., Castor, J. I., & Rybicki, G. B. 1988, *ApJ*, 335, 914
- Owocki, S. P. & Cohen, D. H. 2001, *ApJ*, 559, 1108
- Owocki, S. P., Gayley, K. G. & Shaviv, N. J. 2004, *ApJ*, 616, 525
- Owocki, S. P. & Rybicki, G. B. 1984, *ApJ*, 284, 337
- Runacres, M. C. & Owocki, S. P. 2002, *A&A*, 381, 1015
- ud-Doula, A., & Owocki, S. P. 2002, *ApJ*, 576, 413